JACS
JOURNAL OF THE AMERICAN CHEMICAL SOCIETY
Article
pubs.acs.org/JACS

Tuning of Thermal Stability in Layered $Li(Ni_xMn_yCo_z)O_2$

Jiaxin Zheng,[†,▽] Tongchao Liu,[†,▽] Zongxiang Hu,[†,▽] Yi Wei,[†] Xiaohe Song,[†] Yang Ren,[‡] Weidong Wang,[§] Mumin Rao,[∥] Yuan Lin,[†] Zonghai Chen,[‡] Jun Lu,[‡] Chongmin Wang,[⊥] Khalil Amine,[‡] and Feng Pan*[,†]

[†]School of Advanced Materials, Peking University, Shenzhen Graduate School, Shenzhen 518055, People's Republic of China

[‡]Electrochemical Technology Program, Chemical Sciences and Engineering Division, Argonne National Laboratory, Argonne, Illinois 60439, United States

[§]Shenzhen Tianjiao Technology Development Co., Ltd., Shenzhen 518119, People's Republic of China

[∥]Shenzhen OptimumNano Energy Co., Ltd, Shenzhen 518118, People's Republic of China

[⊥]Environmental Molecular Science Laboratory, Pacific Northwest National Laboratory, 902 Battelle Boulevard, Richland, Washington 99352, United States

Supporting Information

ABSTRACT: Understanding and further designing new layered $Li(Ni_xMn_yCo_z)O_2$ (NMC) ($x + y + z = 1$) materials with optimized thermal stability is important to rechargeable Li batteries (LIBs) for electrical vehicles (EV). Using ab initio calculations combined with experiments, we clarified how the thermal stability of NMC materials can be tuned by the most unstable oxygen, which is determined by the local coordination structure unit (LCSU) of oxygen (TM(Ni, Mn, Co)$_3$-O-Li$_{3-x'}$): each O atom bonds with three transition metals (TM) from the TM-layer and three to zero Li from fully discharged to charged states from the Li-layer. Under this model, how the lithium content, valence states of Ni, contents of Ni, Mn, and Co, and Ni/Li disorder to tune the thermal stability of NMC materials by affecting the sites, content, and the release temperature of the most unstable oxygen is proposed. The synergistic effect between Li vacancies and raised valence state of Ni during delithiation process can aggravate instability of oxygen, and oxygen coordinated with more nickel (especially with high valence state) in LSCU becomes more unstable at a fixed delithiation state. The Ni/Li mixing would decrease the thermal stability of the "Ni═Mn" group NMC materials but benefit the thermal stability of "Ni-rich" group, because the Ni in the Li layer would form 180° Ni−O−Ni super exchange chains in "Ni-rich" NMC materials. Mn and Co doping can tune the initial valence state of Ni, local coordination environment of oxygen, and the Ni/Li disorder, thus to tune the thermal stability directly.

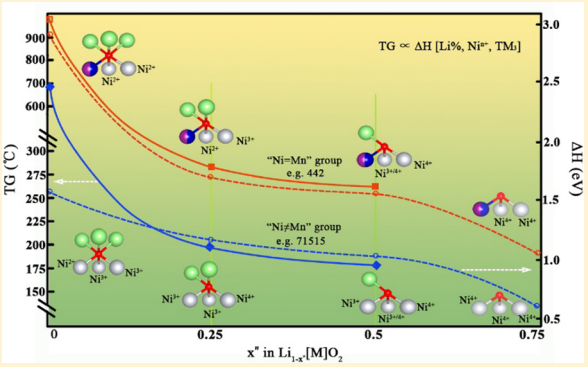

INTRODUCTION

Rechargeable lithium-ion batteries (LIBs) power most of today's portable electronics and are increasingly in demand for electrical vehicles (EV) and grid storages. With this development, major concerns are raised over their safety, cost, and environmental compatibility.[1] For high energy and power density applications (e.g., EVs), the safety becomes especially important. The safety is usually determined by the thermal stability of the cathode materials, which is reflected by the structure decomposition and phase transformation. Generally, the decomposition reaction is accompanied by the oxygen release,[2] which is even more dangerous due to its reaction with the organic electrolytes. Thus, better thermal stability and hard oxygen release in cathode materials are needed for high energy and power density applications of EV LIBs.

As an important cathode material for high-energy-density and EV LIBs, layered $Li(Ni_xMn_yCo_z)O_2$ (NMC, $x + y + z = 1$) materials from solid-solution approaches to $LiMO_2$ (M = Ni, Mn, Co, etc.) have been extensively studied.[3] They not only possess high reversible capacity but also show better Li-ion diffusivity and environmental compatibility than the traditional $LiCoO_2$. However, despite their commercial success, NMC materials usually suffer from poor thermal stability and oxygen release,[2,3b,4] which could decrease the cycling stability and even jeopardize the safety of the batteries. Because NMC materials consist of a closely packed oxygen framework and interstitial metal cations, the oxygen release would cause damage to the structure stability.[4] Using TGA and DSC, Noh et al. studied the impact of the Ni concentration on the thermal stability of these NMC layered oxides.[3b] They found that high Ni content would not benefit for their thermal stability. However, these studies are mainly focused on the impact of Ni content in

Received: July 27, 2016
Published: September 19, 2016

DOI: 10.1021/jacs.6b07771
J. Am. Chem. Soc. 2016, 138, 13326−13334

$Li(Ni_{1/3}Mn_{1/3}Co_{1/3})O_2$ and Ni-rich NMC materials at a fixed state of charge (SOC) = 0.75, such as $Li(Ni_{0.5}Mn_{0.3}Co_{0.2})O_2$, $Li(Ni_{0.6}Mn_{0.2}Co_{0.2})O_2$, $Li(Ni_{0.7}Mn_{0.15}Co_{0.15})O_2$, $Li(Ni_{0.8}Mn_{0.1}Co_{0.1})O_2$, and $Li(Ni_{0.85}Mn_{0.075}Co_{0.075})O_2$. The mechanism for the experimental observations was not discussed in detail yet. Actually, except for the Ni content, the valence state of Ni, the contents of Mn and Co, the lithium content, and the Ni/Li disorder all contribute to the thermal stability of NMC layered oxides. The Ceder group studied the thermal stability of layered oxides theoretically to mainly focus on the charged Li_xNiO_2 and Li_xCoO_2 and calculated their phase stability diagrams to give the detailed phase transition and decomposition process during delithiation or heating process.[2] They reported that the decomposition processes were accompanied by the release of oxygen and then proposed that the thermodynamically driven onset temperature of O_2 gas release could be determined by calculating the entropy for oxygen gas in the reaction. However, they ignored the other factors (e.g., the Ni content, the valence state of Ni, the contents of Mn and Co, and the Ni/Li disordering) that would affect the thermal stability of NMC materials. The Dahn group began to study the thermal stability of layered materials by experimental methods very early. In their 1994 work,[5] using TGA and mass spectrometry, they studied the thermal stability of Li_xCoO_2 and Li_xNiCo_2 and found that nickel materials were not as stable as cobalt materials. Then using accelerating rate calorimetry (ARC), they studied the doping effect on the thermal stability of $LiCoO_2$[6] and $Li(Ni_{1/3}Mn_{1/3}Co_{1/3})O_2$.[7] They found that Mn doping could improve the thermal stability of $LiCoO_2$, but Mg cannot, and Al doping could improve the thermal stability of $Li(Ni_{1/3}Mn_{1/3}Co_{1/3})O_2$, but Mg and Zr cannot. Using ARC, they gave a comparison of the thermal stability of delithiated $Li(Ni_{1/3}Mn_{1/3}Co_{1/3})O_2$, $Li(Ni_{0.8}Co_{0.15}Al_{0.05})O_2$ (NCA), and $LiCoO_2$ in nonaqueous electrolyte and found that $Li(Ni_{1/3}Mn_{1/3}Co_{1/3})O_2$ showed the best thermal stability.[8] Thus, they mainly focused on the doping effect on the thermal stability of $LiCoO_2$ and $Li(Ni_{1/3}Mn_{1/3}Co_{1/3})O_2$ and did not give a systematic study of the tuning factors of the thermal stability for NMC materials yet. Using synchrotron-based time-resolved (TR) X-ray diffraction (XRD) and in situ mass spectroscopy (MS), the Yang group did extensive experimental works on the thermal stability of NMC materials and mainly focus on the detailed structure changes and gas evolution during thermal decomposition of charged $LiNiO_2$,[9] $Li(Ni_{1/3}Mn_{1/3}Co_{1/3})O_2$, and NCA.[10] They found that there was a close correlation between the structure change and the loss of oxygen during heating. They later studied the structure change and thermal stability on charged $Li_{0.34}(Ni_{0.4}Mn_{0.3}Co_{0.3})O_2$, $Li_{0.29}(Ni_{0.5}Mn_{0.3}Co_{0.2})O_2$, $Li_{0.27}(Ni_{0.6}Mn_{0.2}Co_{0.2})O_2$, and $Li_{0.22}(Ni_{0.8}Mn_{0.1}Co_{0.1})O_2$ and found that the content of Ni, Co, and Mn affected both the structural changes and the oxygen release features during heating and that more Ni content would lead to lower onset temperature of thermal decomposition and larger amount of oxygen release,[4] similar to the results reported by Noh et al.[3b] However, they mainly focused on Ni-rich NMC materials and did not consider the "Ni═Mn" NMC materials $[Li[Ni_{0.5}Mn_{0.5}]_{1-x}Co_xO_2$ $(0 < x \leq 0.33)]$[3c] and other factors (e.g., the charge process, the valence state of Ni, and the Ni/Li disordering). Thus, a systematic study and a microscopic picture about all the factors (Ni content, the valence state of Ni, the contents of Mn and Co, the lithium content, and the Ni/Li disordering) to tune the thermal stability of NMC materials are still lacking.

In our previous works, we found that the state of charge and the content of Ni, Co, and Mn can tune the Li-ion diffusivity in layered NMC materials.[11] Hereto, similar questions have been aroused: How do the three transition metals (TMs) and their contents with related valences affect the thermal stability in the layered NMC materials? How can the thermal stability in layered NMC materials be tuned? Thus, a detailed in-depth study is also needed, which would provide important insight toward the understanding of thermal stability in NMC materials and serve as guidelines for future design of improved thermal stability for LIBs.

Herein, using ab initio calculations combined with experiments, we investigate how the thermal stability can be tuned in NMC materials. We divide the NMC materials into two groups: "Ni-rich" group with a mixed valence states of Ni^{2+}/Ni^{3+} and "Ni═Mn" group with only Ni^{2+} state, which will facilitate the systematic study. It is found that the thermal stability is closely correlated to the most unstable oxygen, which is determined by the local coordination structure unit (LCSU): TM(Ni, Mn, Co)$_3$-O-$Li_{3-x'}$ ($x' = 0-3$). The lithium content, valence states of Ni, contents of Ni, Mn, and Co, and Ni/Li disordering can tune the thermal stability of NMC materials by affecting the sites, content, and the release temperature of the most unstable oxygen. During the delithiation process, synergistic effect between Li vacancies and raised valence of Ni formed can aggravate the instability of oxygen, but this effect contributes little to the thermal stability at the medium delithiation state (e.g., from 25% to 50% content of delithiation) for all NMC materials. At a fixed delithiation state, oxygen coordinated with more nickel (especially with high valence state) is more unstable than other kinds of coordination. The Ni/Li mixing would decrease the thermal stability of the "Ni═Mn" group but benefit the thermal stability for "Ni-rich" group, because the Ni in the Li layer would form 180° Ni−O−Ni super exchange chains in Ni-rich NMC materials. The consistency of the theoretical results and experimental results in this work supports the rationality of this simple model, which not only considers all of the impact factors but also provides an easy and direct understanding of the thermal stability of NMC materials from the atomic levels.

EXPERIMENTAL METHODS

Ab Initio Computational Details. All calculations are performed using the plane-wave projector-augmented wave method,[12] as implemented in the Vienna ab initio simulation package.[13] The Perdew−Burke−Ernzerhof (PBE)[14] form of generalized gradient approximation (GGA) is chosen as the exchange−correlation potential. To account for the strong on-site Coulomb interaction (U) presented in the localized 3d electrons of Mn, Co, and Ni, structural properties and electronic properties are calculated by the PBE+U approach[15] with spin polarization, with U values of Mn, Co, and Ni being set at 3.5, 3.3, and 6.4 eV, respectively. These U values are adopted according to the simulation parameters of $Li(Ni_xMn_yCo_z)O_2$ models from the Materials Project Web site (www.materialsproject.org) and our own tests.[11b] Recent studies reported that for some kinds of TM oxides as cathode materials (e.g., Li_8ZrO_6),[16] applying U to p orbitals of oxygen during charging can give a correct picture of oxygen polaron but that PBE cannot. We tested and applied U (1 eV) to p orbitals of oxygen for (333) at SOC = 0.33 and 0.66, respectively. The average magnetic moment of oxygen is reduced from 0.046 to 0.038 at SOC = 0.33 and from 0.069 to 0.057 at SOC = 0.66, respectively. So setting U for oxygen can also correct oxygen polaron for NMC materials. However, different from oxygen

DOI: 10.1021/jacs.6b07771
J. Am. Chem. Soc. 2016, 138, 13326−13334

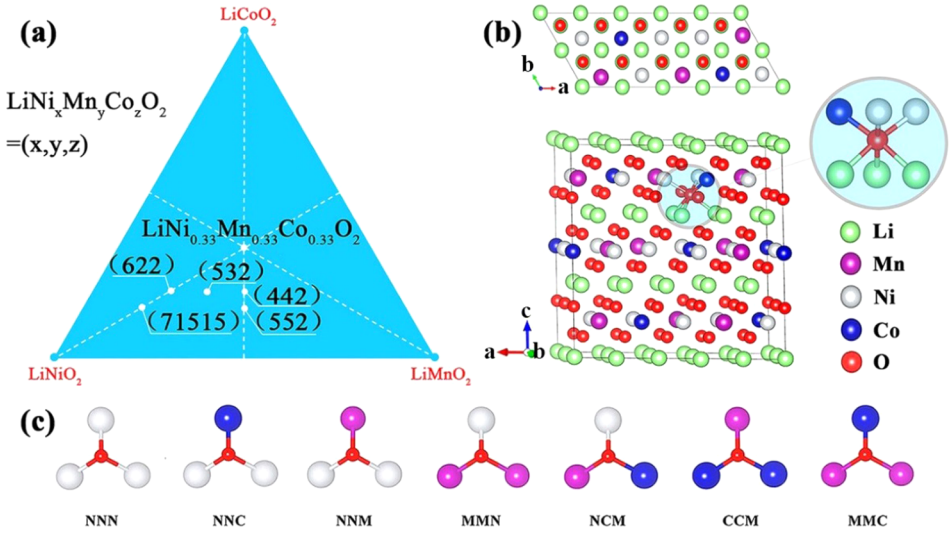

Figure 1. (a) The triangle shows the studied NMC materials. (b) Top view and side views of the structure model of (532). The inset shows the LCSU of oxygen in NMC materials. (c) Seven groups of LCSU for oxygen in NMC materials.

2p orbitals in Li_8ZrO_6 that contribute to the top of the valence bands, oxygen 2p orbitals in NMC materials contribute little to the top of the valence bands during charging, as can be seen from the small magnetic moment for oxygen even at SOC = 0.66. So the correction can be neglected for NMC materials. The small elevation of average magnetic moment of oxygen from SOC = 0.33 to 0.66 can be attributed to the oxidization of cobalt during charging, because the average magnetic moment of oxygen at SOC = 0 is 0.062 and very close to 0.069 at SOC = 0.66.

Layered NMC materials are frequently reported to crystallize in the hexagonal structure with $R\bar{3}m$ space group symmetry.[4,10a] The $C2/m$ space group is only observed at low temperatures (10 K) by the neutron diffraction in $LiNiO_2$, with a slight monoclinic distortion from $R\bar{3}m$ space group symmetry.[17] Thus, all structures built in this work are layered structures with space group $R\bar{3}m$, as the α-$NaFeO_2$ model. The cutoff energy for plane wave is 450 eV.[4] K-points for sampling in Brillouin zone are between 4 × 4 × 2 and 6 × 6 × 2 according to the scale of the reciprocal lattice in our first-principle calculation models. To obtain reliable optimized structures and the total energy, all the atomic positions and cell parameters are fully relaxed. The maximum residual force is <0.01 eV/Å, and energies are converged to within 1×10^{-4} eV per atom. The calculated cell parameters also agree well with the experimental results and previous theoretical results (Table S1), according to a previous report.[18] We apply an antiferromagnetic structure in our NMC layered structure to relax the lattice and calculate structural properties instead of other magnetic structures. The arrangement of Ni, Co, and Mn atoms would affect the total energy of the cell, and it has a relatively large possibility of arrangement in (333), (442), (532), etc. Here we adopt a simplified model, in which the TM atoms are arranged with certain ordering in the compounds.[4] Various experiments and calculations show that the TM compounds exhibit some kind of ordering,[19] such as flower or honeycomb ordering in $Li(Ni_{0.5}Mn_{0.5})O_2$. Taking 622 as an example, we calculated two random distribution structures, and the calculated lattice parameters (a, b, and c) are 5.730, 12.436, 14.021 Å and 5.740, 12.385, 14.017 Å, respectively. The energy of the former is −659.094 eV, and the latter is −659.424 eV. Comparing the lattice parameters to the ordered structure whose lattice constants, a, b, and c, are 5.781 Å, 12.382 Å, and 14.100 Å, respectively, we can find the difference is not significant. But the ordered structure has an obviously lower energy, −661.157 eV. Thus, in our calculations, different ordering of TM ions in $Li(Ni_xMn_yCo_z)O_2$ has been tried to determine the ions arrangement in the slab. As all the ions in NMC layered structure are fully relaxed to the minimum energy, the lattice in our model is the most stable and energetically favorable structure.

Materials Synthesis. Spherical $[Ni_xMn_yCo_z](OH)_2$ precursors (x = 1/3, 0.4, 0.42, 0.5, 0.6, 0.7) were synthesized via the coprecipitation method. The appropriate amounts of $NiSO_4{\cdot}6H_2O$, $CoSO_4{\cdot}7H_2O$, and $MnSO_4{\cdot}5H_2O$ were used as the starting materials for the synthesis of $[Ni_xMn_yCo_z](OH)_2$. An aqueous solution of $NiSO_4{\cdot}6H_2O$, $CoSO_4{\cdot}7H_2O$, and $MnSO_4{\cdot}5H_2O$ with a concentration of 2.0 mol L^{-1} was pumped into a continuously stirred tank reactor (CSTR, 4 L) under a N_2 atmosphere. Concurrently, a 4.0 mol L^{-1} NaOH solution (aq.) and the desired amount of NH_4OH solution (aq.) as a chelating agent were separately pumped into the reactor. Finally, the concentration of the precursor solution is 0.5 mol/L, the pH value of the precursor solution is kept at 10, the temperature is kept at 60 °C, and the stirring speed is kept at 400 rpm/s. The precursor powders were obtained through filtering, washing, and drying in a vacuum oven overnight. $Li(Ni_xMn_yCo_z)O_2$ (x = 1/3, 0.4, 0.42, 0.5, 0.6, and 0.7) were prepared by thoroughly mixing the precursor $[Ni_xMn_yCo_z](OH)_2$ with $LiOH{\cdot}H_2O$ followed by calcination at various temperatures for 15 h: 950 °C for $Li(Ni_{1/3}Mn_{1/3}Co_{1/3})O_2$, 900 °C for $Li(Ni_{0.4}Mn_{0.4}Co_{0.2})O_2$, 900 °C for $Li(Ni_{0.42}Mn_{0.42}Co_{0.16})O_2$, 850 °C for $Li(Ni_{0.5}Mn_{0.3}Co_{0.2})O_2$, 800 °C for $Li(Ni_{0.6}Mn_{0.2}Co_{0.2})O_2$, and 780 °C for $Li(Ni_{0.7}Mn_{0.15}Co_{0.15})O_2$. As the disorder of Li/Ni increases with the increasing ratio of Ni/Co in the same temperature, high temperature increases the disorder of Li/Ni for a fixed ratio of Ni/Co.[3c] Based on these rules, compared with low ratio of Ni/Co such as $Li(Ni_{1/3}Mn_{1/3}Co_{1/3})O_2$ and $Li(Ni_{0.4}Mn_{0.4}Co_{0.2})O_2$, we reduced the sintering temperature of the high ratio of Ni/Co to achieve the similar Li/Ni disorder content. Figure S1 shows the SEM images for all samples. In order to simplify the writing, we named $Li(Ni_{1/3}Mn_{1/3}Co_{1/3})O_2$ as (333), $Li(Ni_{0.4}Mn_{0.4}Co_{0.2})O_2$ as (442), $Li(Ni_{0.42}Mn_{0.42}Co_{0.16})O_2$ as (552), $Li(Ni_{0.5}Mn_{0.3}Co_{0.2})O_2$ as (532), $Li(Ni_{0.6}Mn_{0.2}Co_{0.2})O_2$ as (622), and $Li(Ni_{0.7}Mn_{0.15}Co_{0.15})O_2$ as (71515), respectively. (442), (532), and (622) represent the integer ratio of Ni:Mn:Co in samples $Li(Ni_{0.4}Mn_{0.4}Co_{0.2})O_2$, $Li(Ni_{0.5}Mn_{0.3}Co_{0.2})O_2$, and $Li(Ni_{0.6}Mn_{0.2}Co_{0.2})O_2$, respectively, and they add up to 10. (333) also represents the integer ratio of Ni:Mn:Co in $Li(Ni_{1/3}Mn_{1/3}Co_{1/3})O_2$, but it does not add up to 10. (552) represents the simplest integer ratio of Ni:Mn:Co in $Li(Ni_{0.42}Mn_{0.42}Co_{0.16})O_2$. (71515) represents the NMC sample $Li(Ni_{0.7}Mn_{0.15}Co_{0.15})O_2$ and is just a common notation.

Preparation of Delithiated Positive Electrode Materials. Chemical delithiation of the $Li(Ni_xMn_yCo_z)O_2$ materials was achieved by stirring the powders in acetonitrile solutions containing NO_2BF_4 oxidizer in excess. The molar ratio of NMCs and NO_2BF_4 is 5:2 for SOC = 0.25 and 5:4 for SOC = 0.5, respectively. After 24 h of lithium extraction at room temperature, the $Li(Ni_xMn_yCo_z)O_2$ powders were washed with acetonitrile several times, and the solutions were removed by centrifugation. The resulting materials were then dried at 80 °C

DOI: 10.1021/jacs.6b07771
J. Am. Chem. Soc. 2016, 138, 13326−13334

under vacuum for 24 h and thereafter were stored inside an argon-filled glovebox. Inductively coupled plasma (ICP) was used to analyze the remaining lithium content of $Li_{1-c}(Ni_xMn_yCo_z)O_2$ after chemical delithiation (Table S8). From the SEM images and XRD measurements of the chemical delithiated $Li(Ni_xMn_yCo_z)O_2$ materials (Figures S2 and S3), we can see that compared with the initial samples, there is no obvious change in the morphologies, and they still keep the O3-type layered structure after chemical delithiation. With the increase of delithiation content, the 2θ of 003 of $Li_{1-c}(Ni_xMn_yCo_z)O_2$ moved to the low angle, indicating the increasing interlamellar spacing. The c parameter increases initially with decreasing lithium content due to an increasing electrostatic repulsion across the van der Waals gap between the $Ni_xMn_yCo_zO_2$ layers.

TGA and in Situ XRD Measurements with the Increasing Temperature at Different Delithiation States. Thermal gravimetric analysis (TGA) was conducted under a Ar atmosphere flow for the chemically delithiated $Li_{1-c}(Ni_xMn_yCo_z)O_2$ powders that were placed inside platinum pans, and an empty platinum pan was used as the reference pan. The data were collected using a Seiko Exstar 6000 instrument at a scan rate of 10 °C min^{-1} within the temperature range of 25−900 °C. The in situ XRD data were collected at Bruker D8 Advance diffractometer with Cu Kα (λ = 0.15418 nm), with synchronous heating test function. Approximately 0.2 mg of the NMC samples were loaded onto the sample stage to be heated. In situ XRD patterns (the 2θ range of 10−80° with a step of 0.02° and a count time of 0.2 s for each XRD scan under vacuum conditions) were collected in a continuous manner as the sample was heated from room temperature to 300 °C (i.e., at a heating rate of ∼10 °C min^{-1}).

High-Energy X-ray Diffraction. The high-energy X-ray diffraction (HEXRD) data for the cathode materials were collected at sector 11-ID-C of Advanced Photon Source at Argonne National Laboratory. The wavelength of the X-ray source is 0.111798 Å. Rietveld refinement of the collected HEXRD patterns was carried out using the GSAS package.

RESULTS AND DISCUSSION

The $Li(Ni_xMn_yCo_z)O_2$ materials with TM proportion (x:y:z) = (333), (442), (532), (552), (622), and (71515) were studied here[20] (Figure 1a). Due to the charge redistribution, the oxidation state of TMs in the NMC system (Ni^{2+}, Ni^{3+}, Co^{3+}, Mn^{4+}) is different from that in $LiMO_2$ (M = Ni^{3+}, Co^{3+}, Mn^{3+}).[3c] The Ni participates in the redox behavior, acting as a double redox-active center[21] with $Ni^{2+} \rightarrow Ni^{3+} \rightarrow Ni^{4+}$, and Table S2 shows the proportions of $Ni^{2+}/Ni^{3+}/Ni^{4+}$ in different NMC materials at different delithiation states. Similar to our last work,[11] according to the initial valence state of Ni, we also divide the studied NMC materials into two groups: one group includes (532), (622), and (71515), which can be considered as $LiNiO_2$-substituted solid solutions and named as "Ni-rich" group, and the Ni ions show a mixed valence state of Ni^{2+}/Ni^{3+}. The other group includes (333), (442), and (552), which is named as "Ni═Mn" group and can be considered as a solid solution of $Li(Ni_{0.5}Mn_{0.5})O_2$ and $LiCoO_2$,[3c] and all the Ni ions show the Ni^{2+} state. The representative supercell model of (532) sample is shown in Figure 1b, and all the supercell models of other NMC samples are the same as those demonstrated in our last work,[11] which are also the most energy stable structures. From the perspective of practical applications, here we first mainly focus on the oxygen release, which is also the most important factor to determine the thermal stability and safety for NMC materials.

For the general O_2 release reaction of NMC materials, formation of an oxygen vacancy can be expressed as follows:[2,22] $Li_xTMO_2 \rightarrow Li_xTMO_{2-\Delta} + \Delta/2O_2$. The entropy of solids and the effects of the PV were neglected to compare with entropy of O_2.[22] The reaction entropy change ΔS is contributed by oxygen gas released. The reaction Gibbs free energy can be approximately expressed by[2,22]

$$\Delta G \approx \Delta H - T\Delta S \approx -E^0(Li_xTMO_2) + E^0(Li_xTMO_{2-\Delta}) + \Delta/2E^*(O_2) - T\Delta S$$

where E^0 is total energy at 0 K. The room-temperature enthalpy of O_2 was determined to be −8.95 eV/formula unit.[22] According to JANAF thermochemical tables, the formation temperature of oxygen vacancy can be calculated.[2,22] The inset in Figure 1b shows the LCSU in NMC materials, in which one oxygen connects three Li-ions in Li layer side and three TMs in TM layer side, indicated as TM(Ni, Mn, Co)$_3$-O-$Li_{3-x'}$ (x' = 0−3). To simplify our study, we divide the LCSU into seven groups: NNN, NNC, NNM, NMM, NCM, CCM, and CMM (Figure 1c). Thus, the formation enthalpy (ΔH) of an oxygen vacancy can be finally expressed as ΔH = H(Li%, Ni^{n+}, TM_3), where Li%, Ni^{n+}, and TM_3 are the lithium content, valence state of Ni, and LCSU group, respectively. It should be noted that according to the combination of three TMs (Ni, Mn, and Co) in the LCSU, there should be 10 LCSU groups, but the remaining LCSU groups of MMM, CCC, and CCN do not exist in the most stable and energetically favorable structures of the six kinds of NMC samples from our calculations.

Formation energies of oxygen vacancies at various positions under different states of charge (SOC = 0, 0.25, 0.5, and 0.75) in all NMC materials were calculated, as shown in Tables S3−S6. We first observe that at a fixed SOC, NNN site is most energy favorable for an oxygen vacancy formation in all NMC materials, as it has the smallest formation energy. Note that NNN oxygen only exists in (622) and (71515) materials in our models, while the probability of NNN oxygen existence in other samples is very small. Compared with NNN oxygen, oxygen in NNC or NNM is relatively more stable, indicating harder formation of corresponding vacancies. The rest of the species of oxygen vacancies are comparatively energy unfavorable, as they have higher formation energies. On the other hand, for a fixed TM_3 group (e.g., NCM group in all samples), the formation energy of oxygen vacancy generally decreases with increasing extent of delithiation (Tables S3−S6), indicating that the charge process would lead to easier oxygen release and cause safety problems. It also should be noticed that for a fixed TM_3 group (e.g., NCM group, except for CCM and MMC) and SOC (e.g., SOC = 0), the formation energies of oxygen vacancy in the "Ni═Mn" group are generally larger than that in the "Ni-rich" group (Table S3), which means that oxygen vacancy formation near Ni with a high valence state (Ni^{3+}) in the "Ni-rich" group is easier than that near Ni with a low valence state (Ni^{2+}) in the "Ni═Mn" group. All of the above results indicate that compared to Co^{3+} and Mn^{4+}, oxygen near Ni (Ni^{2+}, Ni^{3+}, and Ni^{4+}) is always unstable. The delithiation process and high valence states of Ni would not benefit from the oxygen stability.

Based on above calculations, we then take (442) and (71515) as two representative samples and propose how the thermal stability evolves in NMC materials at different delithiation states (Figure 2). Here we only consider the most unstable oxygen in both samples (NNC and NNM for (442); NNN for (71515)), because it determines the temperature at which the oxygen starts to release. It can be first seen that the ΔH of oxygen vacancy at the most unstable site decreases with the increasing delithiation in both samples. This can be explained as with the Li-ion being extracted, Li-ion

DOI: 10.1021/jacs.6b07771
J. Am. Chem. Soc. 2016, 138, 13326−13334

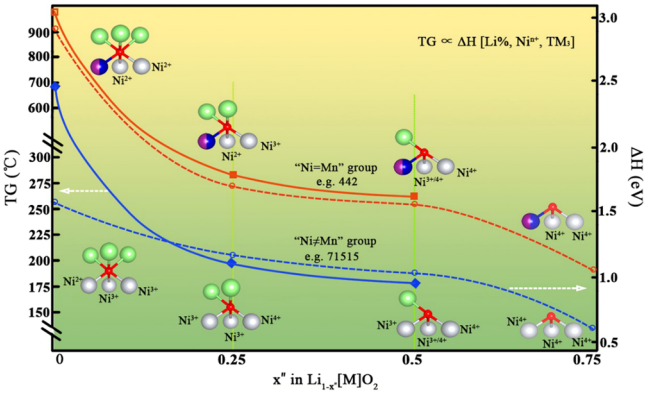

Figure 2. A global view of tuning of thermal stability in a delithiation process. TG: the temperature of the first stage of oxygen loss. ΔH: the calculated oxygen vacancy formation energies at the most unstable LCSU. Green, Li; red, O; silver, Ni; purple, Mn; and blue, Co.

vacancies were formed, from a "single vacancy" unit (TM_3-O-$Li_{3-x'}$, $x' = 1$) at the early delithiation state to "di-vacancy" unit ($x' = 2$) at the medium stage and even "tri-vacancy" unit ($x' = 3$) at overcharged state, as shown in Figure 2, thus leading to the weakened coordination for oxygen. Meanwhile, the oxidation of Ni to high valence states during delithiation would also decrease the ΔH of oxygen vacancy. Interestingly, compared with the sharp variation of ΔH at the early stage and the overcharged state of delithiation, the ΔH stays nearly unchanged at the medium delithiation state (e.g., from 25% to 50% content of delithiation) for all samples, indicating the variation of Li-ion content and the valence state of Ni contributes little to the ΔH of oxygen vacancy at the normal charged state, and it is a safe range to charge battery. Our TGA measurements of the temperature of the first stage of oxygen loss (TG) for all NMC samples also shows the same trend as the theoretical prediction (Figure 2). Note that each sample nearly shows the same TG at $x'' = 0.25$ and 0.5. However, compared with 25% delithiation, the sample with 50% delithiation shows more weight loss (Figure S8), indicating more of the most unstable oxygen at the more delithiated state.

Furthermore, combining the calculated formation energies of oxygen vacancy and TGA measurements, we studied how the different contents of Ni, Co, and Mn and their valence states tune the thermal stability in NMC materials. Table S18 summarizes the type of the most unstable oxygen, TG, and the oxygen release content at the first stage of weight loss in all NMC materials at different SOC. The calculated ΔH of oxygen vacancies with different LCSUs and the measured TG in all NMC materials at SOC = 0.5 are compared in Figure 3a,b, and both ΔH of oxygen vacancy at the most unstable site and TG show the same trend. For "Ni-rich" group, the experimental TG decreases with the increasing Ni content, in accordance with previous works.[3b,c,4] According to the calculations, higher contents and valence states of Ni would lead to small ΔH for oxygen vacancy. Thus, though (622) and (71515) contain the same most unstable NNN group of oxygen vacancies, the TG of (71515) is a little lower than that of (622), because the Ni^{4+} content in (71515) with 35% is a little higher than that in (622) with 30% at SOC = 0.5 (Table S2). Meanwhile, the most unstable oxygen in (532) is the NNM type, which is more stable than the NNN type, leading to the highest TG in "Ni-rich" group. For "Ni=Mn" group, their TG values are all much higher than those of "Ni-rich" group. For example, (71515) and (622) show the lowest TG around 180 °C, while (333) and (552) show TG around 300 °C at SOC = 0.5. This can be mainly attributed to that there is no NNN type oxygen vacancy in "Ni=Mn" group. Another reason is the relatively low content of high valence state of Ni (e.g., Ni^{4+}) in "Ni=Mn" group. For example, at SOC = 0.5, the Ni^{4+} content in (532) is 20%, which is higher than that in all "Ni=Mn" samples (8% ∼ 17%). Thus, the oxygen at NNM or NNC positions in (532) sample is obviously less stable compared with oxygen at the same NNM or NNC positions in all "Ni=Mn" samples. Especially, the types of the most unstable oxygen for (442) and (532) are both NNC, but the ΔH for NNC type oxygen vacancy in (532) is smaller than that for (442). Interestingly, the types of the most unstable oxygen in (333), (442), and (552) samples are NCM, NNC, and NNM, respectively, depending on the mole ratios of Ni, Co, and Mn. The ΔH for oxygen vacancy at NCM, NNC, and NNM follows the order: ΔH(NCM) > ΔH(NNM) > ΔH(NNC), and the TG for (333), (442), and (552) samples also confirms this trend. Finally, from the TGA measurements, we can see that the weight loss (oxygen release content) of the first stage in "Ni-rich" group is also heavier than those in the "Ni=Mn" group (Table S18), consistent with the trends of TG and ΔH.

Ni/Li mixing usually happens in NMC materials.[3c] We further considered the impact of Ni/Li disorder on the thermal stability (Figure 4). The content of Ni/Li disorder in all samples is estimated by Rietveld refinement of the XRD data

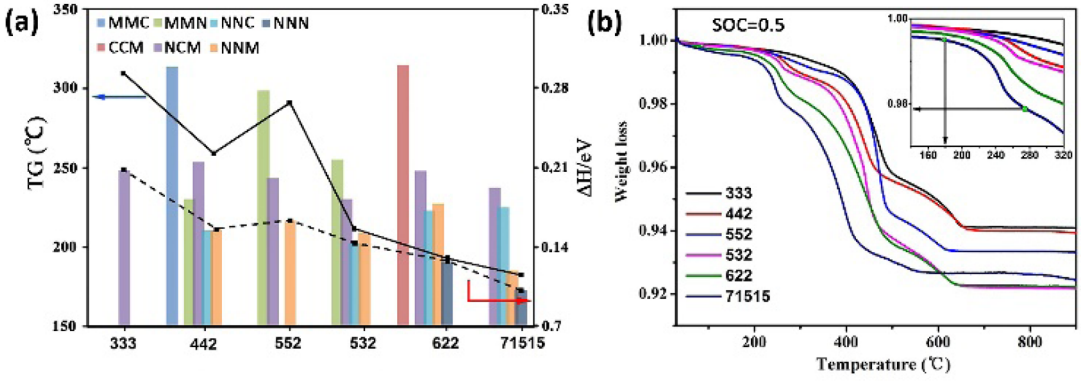

Figure 3. (a) Comparison of TG and the calculated ΔH of oxygen vacancy at the most unstable LCSU at SOC = 0.5. (b) TGA curves of the chemically delithiated $Li_{1-x''}(Ni_xMn_yCo_z)O_2$.

DOI: 10.1021/jacs.6b07771
J. Am. Chem. Soc. 2016, 138, 13326−13334

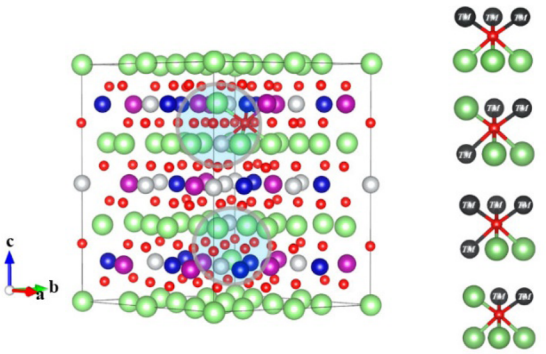

Figure 4. Structure model of (333) with a content of 6.67% for Ni/Li mixing. The right panel shows four representative LCSUs of oxygen in a supercell without and with Ni/Li disordering.

(Figure S4). As shown in Table S16, we can see that the contents of Ni/Li disorder for all the samples are similar, with a proportion within the range of 4.5%−5.5%. To get more accurate results, the structure properties for samples of (442), (532), (622), and (71515) are further measured by using HEXRD (Figure S5). As shown in Table S17, the Rietveld refinement results show the contents of Ni/Li disorder in all simples are similar, consistent with the results of XRD. From these two sets of data, we can see that even though the sintering temperatures of each Ni/Co sample were different, all the samples roughly show the similar content of Ni/Li disorder. Table 1 shows the calculated ΔH of oxygen vacancies at different LCSUs for all samples with a content of 6.7% for Ni/Li mixing (this value is convenient for constructing supercells for calculation) at SOC = 0. It can be seen that the Ni/Li mixing indeed affects the thermal stability of NMC materials. For the "Ni═Mn" group, the (ΔH)s at different LCSUs are generally decreased after considering Ni/Li mixing, indicating an easier loss of oxygen. While for "Ni-rich" group, the (ΔH)s at different LCSUs are generally increased after considering Ni/Li mixing, indicating a harder loss of oxygen. The is because after Ni/Li mixing in the "Ni-rich" group, the Ni in the Li layer would form 180° Ni−O−Ni super exchange chains easily,[23] the O ion between the spin parallel Ni forms σ-bonding with one Ni ion, and the O ion between the spin antiparallel Ni forms π-bonding. This would enhance the structure stability for "Ni-rich" NMC materials. Thus, the Ni/Li mixing would benefit from the thermal stability for the "Ni-rich" group but decrease the thermal stability of the "Ni═Mn" group. Considering the ΔH of the most unstable oxygen, the fact that the "Ni═Mn" group shows better thermal stability than the "Ni-rich" group is still unchanged even after taking into account the Ni/Li mixing.

The oxygen release would affect the structure stability by inducing structure expansion and distortion, cation disordering, phase transition, and so on. To further detail the close correlation between the thermal stability and the most unstable oxygen, in situ XRD affords us a good roadmap for the average structural changes[10a] in NMC materials ($R\bar{3}m$) during thermal decomposition in heat process (Figures 5a and S9−S13). Taking (71515) at SOC = 0.5 as an example (Figure 5a), similar to the reported work on (333) and NCA by Nam et al.,[10a] before 160 °C, $(003)_R$ moves to lower 2θ, which was mainly caused by thermal expansion of the material. After 160 °C, $(003)_R$ peaks shift to higher 2θ with increasing temperature. This can be attributed to the decreasing electrostatic repulsion across the van der Waals gap between the $Ni_xMn_yCo_zO_2$ layers with the oxygen loss. Similar to the (71515), other materials also exhibit similar changes, and the difference for them is the temperature of the oxygen starting to release. The $(003)_R$ peaks shift vs temperature for all NMC materials in heat process are shown in Figure 5b. It is found that the shift of $(003)_R$ peaks for (71515) and (622) begins much earlier at about 160 °C, and as the temperature increases, the peaks shift more dramatically. By contrast, there is nearly no shift for $(003)_R$ peaks of (333) before 300 °C. For all NMC materials and on the whole, the results of XRD confirm that "Ni═Mn" group shows better thermal stability than "Ni-rich" group, in accordance with the trends of TGA measurements and the calculated ΔH of oxygen vacancy. Further analysis on in situ XRD data (Figure 5c,d) shows that in addition to the peak shifts, the intensity of $(003)_R$ peaks becomes weaker, and the merging of the $(018)_R/(110)_R$ pairs becomes more serious as the temperature raised. According to the previous report,[10a] the ratio of the integrated intensity of $I(003)/I(104)$ and the merging of the $(018)_R/(110)_R$ pairs are two key parameters reflecting the degree of the mixing of Ni and Li ions. If the integrated intensity of $I(003)/I(104)$ is <1.2 and the $(018)_R/(110)_R$ pairs begin to merge, it means that Ni and Li ion mixing happens. This is because the evolution of oxygen at elevated temperature causes anion vacancies that facilitate the migration of TM ions from the TM layer into the Li layer to form a spinel-like structure, which is kinetically slow without the presence of anion vacancies. From Figure 5c, it can be seen that the ratio of the integrated intensity of $I(003)/I(104)$ decreases with the increasing temperature, indicating that the cation mixing becomes heavier with the increasing oxygen release. Figure S15 shows the curve of $I(003)/I(104)$ vs temperature for all NMC samples. We can see that in the "Ni-rich" group, the variation degree becomes larger with the increasing Ni content, and in "Ni═Mn" group, it follows as (333) < (552) < (442) (Figure S15b). The variation degree for "Ni═Mn" group is also smaller than "Ni-

Table 1. Formation Energies of Oxygen Vacancies (ΔH) at Different LCSUs for all Samples with 6.67% Content of Ni−Li Antisite Disordering at SOC = 0

	ΔH of Oxygen Vacancies at Different LCSUs (eV)							
compd	NNN	NNM	NNC	NCM	MMN	CCM	MMC	O-anti
(333)	–	–	–	3.58	–	–	–	3.66
(442)	–	–	2.69	2.94	2.73	–	3.83	2.94
(552)	–	4.11	–	3.44	2.13	–	–	3.26
(532)	–	2.13	2.43	2.71	–	–	–	2.71
(622)	2.25	2.61	2.54	3.71	–	3.24	–	2.04
(71515)	1.50	2.29	2.53	2.86	–	–	–	1.57

[a]O-anti denotes the most unstable oxygen with Ni/Li disordering in a LCSU, as shown in Figure 4.

DOI: 10.1021/jacs.6b07771
J. Am. Chem. Soc. 2016, 138, 13326−13334

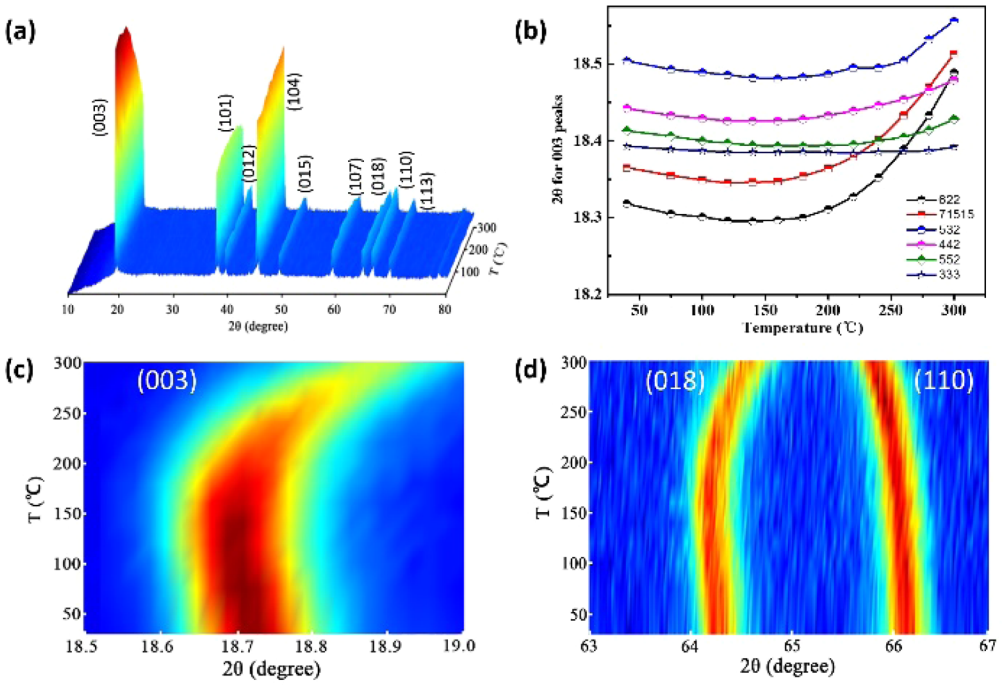

Figure 5. (a) In situ XRD measurements of (71515) at SOC = 0.5 in heat process. (b) $(003)_R$ peaks shift vs temperature for all NMC materials. (c and d) Involution of $(003)_R$ peaks and $(018)_R/(110)_R$ pairs.

rich" group, indicating better thermal stability in "Ni═Mn" group. Thus, all the above variation trends with the Ni content agree well with the TGA measurements and the calculated ΔH of oxygen vacancy (Figure 3a).

From above results, we can see that the contents of Ni, Mn, Co can tune the thermal stability by affecting the local coordination structure of oxygen ($TM(Ni, Mn, Co)_3$-O-$Li_{3-x'}$). Doping Mn^{4+} and Co^{3+} can contribute to stabilizing oxygen, because compared with Ni^{2+} and Ni^{3+}, the d band moves up in energy for Mn^{4+} and Co^{3+}, the filling of e_g band decreases, and the antibonding oxygen−metal d states become more depopulated (Figure S16), resulting in stronger bonding for Mn−O and Co−O. Oxidation of Ni^{2+} and Ni^{3+} to Ni^{4+} would decrease the oxygen stability, which can be attributed to the increased Coulomb repulsion among the three TM cations in $TM(Ni, Mn, Co)_3$ and the harder to get electron from e_g band of Ni for oxygen. Besides, the content of Co^{3+} can stabilize the Ni^{2+} in the TM layer to suppress the cation disordering,[3c] and the increased content of Mn^{4+} can push the valence state of some Ni atoms from Ni^{3+} to Ni^{2+} to stabilize the oxygen. Meanwhile, the invariant Mn^{4+} in NMC materials also helps to stabilize the layered structure and protects them from the spinel-like phase transition or any Jahn−Teller distortion of (Mn^{3+}).[3c] These findings reveal that we can tune the thermal stability of NMC materials not only by changing the contents of Ni, Mn, and Co but also by doping other elements to change the local coordination structure of oxygen or to act the similar role as Mn or Co does.

Finally, previous studies report that besides the intrinsic thermal stability of the bulk, the surface composition and structure of NMC materials are different from the bulk and also play an important role on the thermal behaviors of the layered NMC materials during electrochemical cycling.[24] This role is mainly reflected from three aspects: one aspect is that for the normal pristine NMC sample with the layered structure from bulk to surface (the well-synthesized pristine NMC samples before electrochemical cycling generally exhibit a well-defined ($R\bar{3}m$) crystal structure with a homogeneous distribution of the electronic structure),[10a,24c] due to the trunked symmetry at the surface, the LCSU of oxygen ($TM(Ni, Mn, Co)_3$-O-Li_3) was broken at the surface. Thus, compared with the oxygen in the bulk NMC materials, the surface oxygen becomes unsaturated and more unstable, and oxygen evolution would first happen or initiate at the surface during electrochemical cycling. Particularly, if the NMC electrodes are overcharged, according to our calculations, the ΔH at the overcharged state of delithiation would decrease sharply, indicating a much easier oxygen loss at this stage. This would lead to an accelerated TM/Li mixing and phase transformation at the surfaces of NMC cathodes and cause damage to the thermal stability. The second aspect is that Ni-rich NMC pristine samples usually show strong surface segregation of antisite defects (mainly Ni/Li mixing) and Ni toward open facets (surfaces perpendicular to the layered arrangement of atoms)[24a] and even a rock-salt NiO phase,[25] which is attributed to the low Ni migration barriers. Such surface segregation of Ni/Li mixing and surface rock-salt NiO phase would improve the thermal stability of Ni-rich NMC samples and would not benefit from the charge transfer and Li-ion transport at the electrode/electrolyte interface. The third aspect is that the surface of delithated cathodes is extremely reactive due to a substantial overlap between the 3d band of Ni and the 2p band of oxygen, finally leading to the chemical reaction between the charged layered cathode and the nonaqueous electrolyte to form a surface reaction layer.[24c] This is more serious in the Ni-rich NMC materials, because of the more nickel content and the easy oxygen loss. The surface reaction layer is mainly formed during the first cycle and would prevent further reactions between the charged layered cathode and the nonaqueous electrolyte during the later cycles and impede the charge transfer and Li-ion transport at the electrode/electrolyte interface. Besides, for the overdelithiated states under high voltages, the high Ni^{4+} content in the NMC

DOI: 10.1021/jacs.6b07771
J. Am. Chem. Soc. 2016, 138, 13326−13334

electrodes would facilitate the surface chemical evolution by the reactions between the overcharged layered cathode and the nonaqueous electrolyte.[10a] To protect the surface structure stability of NMC materials, various nanocoating methods are developed to serve as a physical barrier between the layered cathode and the electrolyte, such as coating NMC materials with more stable cathode nanoparticles[26] and with oxides by atomic layer deposition.[27]

In summary, both ab initio calculations and the experimental measurements demonstrated the thermal stability is correlated to the most unstable oxygen, which is determined by the oxygen local coordination structure unit ($TM(Ni, Mn, Co)_3$-O-$Li_{3-x'}$). Via this simple model, the factors (the lithium content, valence states of Ni, contents of Ni, Mn, and Co, and Ni/Li disorder) to tune the thermal stability of NMC materials by affecting the sites, content, and the release temperature of the most unstable oxygen are proposed. During charging process, the synergistic effect between Li vacancies and raised valence state of Ni process can aggravate instability of oxygen. For a fixed lithium content, oxygen coordinated with more nickel (especially with high valence state) in the LSCU becomes more unstable, which explains the previous reports that more Ni content would lead to a lower onset temperature of thermal decomposition and a larger amount of oxygen release.[3b,4] The Ni/Li mixing would decrease the thermal stability of the "Ni═Mn" group, but the thermal stability for "Ni-rich" group would benefit, because the Ni in the Li layer would form 180° Ni−O−Ni super exchange chains in Ni-rich NMC materials. Mn and Co doping can tune the thermal stability directly by tuning the initial valence state of Ni, local coordination environment of oxygen, and the Ni/Li disorder. These new insights can serve as design principles for future discovery of improved thermal stability for LIBs. For example, by considering the high thermal stability as well as the fast Li-ion diffusivity and high reversible capacity for "Ni═Mn" group,[11b] we propose that developing a $Li[Ni_{0.5}Mn_{0.5}]_{1-x}Co_xO_2$ ($0 < x \leq 0.33$) system would be a promising way to further optimize the thermal stability of NMC materials with high performance.

■ ASSOCIATED CONTENT

Supporting Information

The Supporting Information is available free of charge on the ACS Publications website at DOI: 10.1021/jacs.6b07771.

Details about tables of relevant lattice parameters, the ratio of $Ni^{2+}/Ni^{3+}/Ni^{4+}$ in different samples at different SOC, and formation energies of oxygen vacancies in various positions at different SOC; figures of XRD, HEXRD, TGA measurements, and in situ XRD data (PDF)

■ AUTHOR INFORMATION

Corresponding Author

*panfeng@pkusz.edu.cn

Author Contributions

▽These authors contributed equally.

Notes

The authors declare no competing financial interest.

■ ACKNOWLEDGMENTS

The work was financially supported by National Materials Genome Project (2016YFB0700600), National Project for EV Batteries (20121110, OptimumNano, Shenzhen), Guangdong Innovation Team Project (no. 2013N080), Shenzhen Science and Technology Research Grant (nos. ZDSY20130331145131323, JCYJ20140903101633318, JCYJ2014090-3101617271). The authors also acknowledge the use of the Advanced Photon Source (APS), which is supported by the U.S. Department of Energy, Office of Science, Office of Basic Energy Science.

■ REFERENCES

(1) Suo, L.; Borodin, O.; Gao, T.; Olguin, M.; Ho, J.; Fan, X.; Luo, C.; Wang, C.; Xu, K. *Science* **2015**, *350*, 938−943.

(2) Wang, L.; Maxisch, T.; Ceder, G. *Chem. Mater.* **2007**, *19*, 543−552.

(3) (a) Goodenough, J. B.; Kim, Y. *Chem. Mater.* **2010**, *22*, 587−603. (b) Noh, H. J.; Youn, S.; Yoon, C. S.; Sun, Y. K. *J. Power Sources* **2013**, *233*, 121−130. (c) Whittingham, M. S. *Chem. Rev.* **2004**, *104*, 4271−4302.

(4) Bak, S. M.; Hu, E. Y.; Zhou, Y. N.; Yu, X. Q.; Senanayake, S. D.; Cho, S. J.; Kim, K. B.; Chung, K. Y.; Yang, X. Q.; Nam, K. W. *ACS Appl. Mater. Interfaces* **2014**, *6*, 22594−22601.

(5) Dahn, J. R.; Fuller, E. W.; Obrovac, M.; Von Sacken, U. *Solid State Ionics* **1994**, *69*, 265−270.

(6) (a) Jiang, J.; Dahn, J. R. *Electrochem. Commun.* **2004**, *6*, 39−43. (b) Lu, Z.; MacNeil, D. D.; Dahn, J. R. *Electrochem. Solid-State Lett.* **2001**, *4*, A200−A203. (c) Luo, W.; Li, X.; Dahn, J. R. *J. Electrochem. Soc.* **2010**, *157*, A993−A1001. (d) Zhou, F.; Luo, W.; Zhao, X.; Dahn, J. R. *J. Electrochem. Soc.* **2009**, *156*, A917−A920.

(7) (a) Luo, W.; Zhou, F.; Zhao, X.; Lu, Z.; Li, X.; Dahn, J. R. *Chem. Mater.* **2010**, *22*, 1164−1172. (b) Zhou, F.; Zhao, X.; Lu, Z.; Jiang, J.; Dahn, J. R. *Electrochem. Commun.* **2008**, *10*, 1168−1171. (c) Luo, W.; Dahn, J. R. *J. Electrochem. Soc.* **2011**, *158*, A428−A433. (d) Zhou, F.; Zhao, X.; Dahn, J. R. *J. Electrochem. Soc.* **2009**, *156*, A343−A347.

(8) Wang, Y.; Jiang, J.; Dahn, J. R. *Electrochem. Commun.* **2007**, *9*, 2534−2540.

(9) (a) Yoon, W.-S.; Hanson, J.; McBreen, J.; Yang, X.-Q. *Electrochem. Commun.* **2006**, *8*, 859−862. (b) Yoon, W.-S.; Chung, K. Y.; Balasubramanian, M.; Hanson, J.; McBreen, J.; Yang, X.-Q. *J. Power Sources* **2006**, *163*, 219−222.

(10) (a) Nam, K. W.; Bak, S. M.; Hu, E.; Yu, X.; Zhou, Y.; Wang, X.; Wu, L.; Zhu, Y.; Chung, K. Y.; Yang, X. Q. *Adv. Funct. Mater.* **2013**, *23*, 1047−1063. (b) Bak, S.-M.; Nam, K.-W.; Chang, W.; Yu, X.; Hu, E.; Hwang, S.; Stach, E. A.; Kim, K.-B.; Chung, K. Y.; Yang, X.-Q. *Chem. Mater.* **2013**, *25*, 337−351. (c) Belharouak, I.; Lu, W.; Vissers, D.; Amine, K. *Electrochem. Commun.* **2006**, *8*, 329−335. (d) Yoon, W.-S.; Balasubramanian, M.; Yang, X.-Q.; McBreen, J.; Hanson, J. *Electrochem. Solid-State Lett.* **2005**, *8*, A83−A86. (e) Nam, K.-W.; Yoon, W.-S.; Yang, X.-Q. *J. Power Sources* **2009**, *189*, 515−518.

(11) (a) Cui, S.; Wei, Y.; Liu, T.; Deng, W.; Hu, Z.; Su, Y.; Li, H.; Li, M.; Guo, H.; Duan, Y. *Adv. Energy Mater.* **2016**, *6*, 1501309. (b) Wei, Y.; Zheng, J. X.; Cui, S. H.; Song, X. H.; Su, Y. T.; Deng, W. J.; Wu, Z. Z.; Wang, X. W.; Wang, W. D.; Rao, M. M.; Lin, Y.; Wang, C. M.; Amine, K.; Pan, F. *J. Am. Chem. Soc.* **2015**, *137*, 8364−8367.

(12) (a) Blöchl, P. E. *Phys. Rev. B: Condens. Matter Mater. Phys.* **1994**, *50*, 17953−17979. (b) Kresse, G.; Joubert, D. *Phys. Rev. B: Condens. Matter Mater. Phys.* **1999**, *59*, 1758−1775.

(13) (a) Kresse, G.; Furthmüller, J. *Phys. Rev. B: Condens. Matter Mater. Phys.* **1996**, *54*, 11169−11186. (b) Kresse, G.; Furthmüller, J. *Comput. Mater. Sci.* **1996**, *6*, 15−50.

(14) Perdew, J. P.; Burke, K.; Ernzerhof, M. *Phys. Rev. Lett.* **1996**, *77*, 3865−3868.

(15) Anisimov, V. I.; Zaanen, J.; Andersen, O. K. *Phys. Rev. B: Condens. Matter Mater. Phys.* **1991**, *44*, 943−954.

(16) (a) Huang, S.; Wilson, B. E.; Smyrl, W. H.; Truhlar, D. G.; Stein, A. *Chem. Mater.* **2016**, *28*, 746−755. (b) Huang, S.; Wilson, B. E.; Wang, B.; Fang, Y.; Buffington, K.; Stein, A.; Truhlar, D. G. *J. Am. Chem. Soc.* **2015**, *137*, 10992−11003. (c) Huang, S.; Fang, Y.; Wang, B.; Wilson, B. E.; Tran, N.; Truhlar, D. G.; Stein, A. *J. Phys. Chem. C* **2016**, *120*, 9637−9649.

(17) Chung, J. H.; Proffen, T.; Shamoto, S.; Ghorayeb, A. M.; Croguennec, L.; Tian, W.; Sales, B. C.; Jin, R.; Mandrus, D.; Egami, T. *Phys. Rev. B: Condens. Matter Mater. Phys.* **2005**, *71*, 064410.
(18) Hwang, B.; Tsai, Y.; Carlier, D.; Ceder, G. *Chem. Mater.* **2003**, *15*, 3676−3682.
(19) (a) Van der Ven, A.; Ceder, G. *Electrochem. Commun.* **2004**, *6*, 1045−1050. (b) Yu, H.; Qian, Y.; Otani, M.; Tang, D.; Guo, S.; Zhu, Y.; Zhou, H. *Energy Environ. Sci.* **2014**, *7*, 1068−1078. (c) Bréger, J.; Kang, K.; Cabana, J.; Ceder, G.; Grey, C. P. *J. Mater. Chem.* **2007**, *17*, 3167−3174. (d) Thackeray, M. M.; Kang, S.-H.; Johnson, C. S.; Vaughey, J. T.; Benedek, R.; Hackney, S. *J. Mater. Chem.* **2007**, *17*, 3112−3125.
(20) (a) Yoon, W.-S.; Grey, C. P.; Balasubramanian, M.; Yang, X.-Q.; McBreen, J. *Chem. Mater.* **2003**, *15*, 3161−3169. (b) Li, D.; Sasaki, Y.; Kobayakawa, K.; Sato, Y. *Electrochim. Acta* **2006**, *51*, 3809−3813. (c) Li, D.; Sasaki, Y.; Kageyama, M.; Kobayakawa, K.; Sato, Y. *J. Power Sources* **2005**, *148*, 85−89. (d) Li, Z.; Chernova, N. A.; Roppolo, M.; Upreti, S.; Petersburg, C.; Alamgir, F. M.; Whittingham, M. S. *J. Electrochem. Soc.* **2011**, *158*, A516−A522. (e) Tran, N.; Croguennec, L.; Jordy, C.; Biensan, P.; Delmas, C. *Solid State Ionics* **2005**, *176*, 1539−1547.
(21) (a) Hwang, B. J.; Tsai, Y. W.; Carlier, D.; Ceder, G. *Chem. Mater.* **2003**, *15*, 3676−3682. (b) Ren, H.; Huang, Y.; Wang, Y.; Li, Z.; Cai, P.; Peng, Z.; Zhou, Y. *Mater. Chem. Phys.* **2009**, *117*, 41−45. (c) Wu, Z. Z.; Han, X. G.; Zheng, J. X.; Wei, Y.; Qiao, R. M.; Shen, F.; Dai, J. Q.; Hu, L. B.; Xu, K.; Lin, Y.; Yang, W. L.; Pan, F. *Nano Lett.* **2014**, *14*, 4700−4706. (d) Yu, H. J.; Qian, Y. M.; Otani, M. R.; Tang, D. M.; Guo, S. H.; Zhu, Y. B.; Zhou, H. S. *Energy Environ. Sci.* **2014**, *7*, 1068−1078.
(22) Kim, Y.; Kim, D.; Kang, S. *Chem. Mater.* **2011**, *23*, 5388−5397.
(23) Chen, H.; Dawson, J. A.; Harding, J. H. *J. Mater. Chem. A* **2014**, *2*, 7988−7996.
(24) (a) Dixit, H.; Zhou, W.; Idrobo, J.-C.; Nanda, J.; Cooper, V. R. *ACS Nano* **2014**, *8*, 12710−12716. (b) La Mantia, F.; Rosciano, F.; Tran, N.; Novák, P. *J. Appl. Electrochem.* **2008**, *38*, 893−896. (c) Lin, F.; Markus, I. M.; Nordlund, D.; Weng, T.-C.; Asta, M. D.; Xin, H. L.; Doeff, M. M. *Nat. Commun.* **2014**, *5*, 3529.
(25) Cho, Y.; Oh, P.; Cho, J. *Nano Lett.* **2013**, *13*, 1145−1152.
(26) Wu, Z.; Ji, S.; Liu, T.; Duan, Y.; Xiao, S.; Lin, Y.; Xu, K.; Pan, F. *Nano Lett.* **2016**, DOI: 10.1021/acs.nanolett.6b02742.
(27) Meng, X.; Yang, X.-Q.; Sun, X. *Adv. Mater.* **2012**, *24*, 3589−3615.

DOI: 10.1021/jacs.6b07771
J. Am. Chem. Soc. 2016, 138, 13326−13334